IEEE Access
Multidisciplinary ⋮ Rapid Review ⋮ Open Access Journal

Received August 24, 2020, accepted August 27, 2020, date of publication September 8, 2020, date of current version September 22, 2020.

Digital Object Identifier 10.1109/ACCESS.2020.3022670

Power Line Simulation for Safety Distance Detection Using Point Clouds

SAI CHANG ZHANG[1,2], JUN ZHENG LIU[3], ZHENG NIU[1], SHUAI GAO[1], HAI ZHI XU[4], AND JIE PEI[5]

[1]Aerospace Information Research Institute, Chinese Academy of Sciences, Beijing 100101, China
[2]University of Chinese Academy of Sciences, Beijing 100049, China
[3]Institute of Photogrammetry and Remote Sensing, Chinese Academy of Surveying and Mapping, Beijing 100036, China
[4]Airborne Patrolling Center of Guangdong Power Grid, China Southern Power Grid, Guangzhou 510000, China
[5]School of Geospatial Engineering and Science, Sun Yat-Sen University, Guangzhou 510275, China

Corresponding author: Sai Chang Zhang (zhangcs@radi.ac.cn)

This work was supported in part by the Program of National Natural Science Foundation of China under Grant 41730107, and in part by the Program of Chinese Academy of Sciences under Grant GF-7 Y8D00400GF.

ABSTRACT Airborne LiDAR has been adopted as a powerful survey tool for overhead power transmission line (TL) cruising so that the operator can quickly search for, locate and eliminate the risk objects at the power line corridor scene. However, the TLs are moving objects, which positions are dynamically affected by working conditions (e.g. temperature variation, wind-induced conductor motion) while they are acquired by airborne LiDAR. The point clouds data acquired by airborne LiDAR only reflect the geometric relationship between the TL and its surrounding objects at the transient moment of the data acquisition. In order to overcome the shortcomings of the instantaneously acquired laser scanning data, this article presents an approach for simulating the dynamic TL shape under different working conditions based on mechanical computation of the overhead line. The proposed approach considers the tension variation of TL resulting from weather conditions, such as temperature, wind and ice, while simulates TL sag curve using the parabolic catenary equation combined with the tension. A performance evaluation was conducted over the TLs data with multiple voltage levels. Experiments results show that the proposed approach is effective for simulating the 3D shape of TL under different working conditions. The simulation error achieved was less than 0.65m and the maximum Diff-Ratio was about 1.57%. This provides a scientifically sound predicting and modeling approach for TL risk assessment and warning along the corridor.

INDEX TERMS Airborne laser scanning, remote sensing, power line modeling, risk management, transmission line simulation.

I. INTRODUCTION

The safety of overhead power transmission line (TL) infrastructure is of importance to the quality of both daily life and industrial activities. High-voltage transmission lines are regarded as the most crucial part of the TL infrastructure. Automated and timely monitoring of high-voltage transmission lines is required for the surveying of transmission line corridors [1]. Generally, there are two components of TL corridor surveys: the analysis of TL structural stability and the detection of potential hazards, especially vegetation [2]. Trees growing close to the TLs can damage the infrastructure and cause widespread electrical failures or bush fires. Therefore, the safety distance must be maintained in order to prevent the occurrence of such incidents [3]. Specifically, it's necessary for regular inspections of vegetation inside and near to the TL corridor to detect and cut the trees or tree branches that dissatisfy safety distance requirements [4], in order to ensure the safe operation of electrical networks [5].

For the last decade, many approaches have been proposed for monitoring and modeling TLs, mainly including field surveys and airborne surveys [6], [7]. The field survey depend on human visual observations using telescopes, which is labour-intensive, inefficient and uneconomical. Airborne survey based on a variety of remote sensing methods for TL monitoring tasks. For example, low-altitude unmanned aerial vehicles (UAV) have been used combined with remote sensing technology in order to monitor TL safety distances [8]. TLs have been documented by aerial images manually or in a semi-automated manner (e.g. using stereo-images) [9], [10]. The general ideas behind the methods which use images to detect the safety distance are basically similar: the

The associate editor coordinating the review of this manuscript and approving it for publication was Qiangqiang Yuan.

three-dimensional (3D) coordinates of the TL and the ground points are extracted first, and then the distance is judged. However, as they are limited by the image quality, scene complexity and stereo-image matching process, the image-based methods are time-consuming and are not sufficiently reliable.

As an alternative to the optical imagery, airborne LiDAR can directly obtain accurate 3D coordinates of the power line scene using laser range data and the precise instantaneous position, and orientation information are acquired by a high-precision Positioning and Orientation System (POS). Pointclouds data that can describe the 3D geometric relationship between corridor objects are then created [11], without the need for the time-consuming stereo-image matching process that is involved when using computer vision and photogrammetry techniques. Therefore, this process can conduct distance detection more effectively than an image-based method. Using airborne laser scanning techniques, a high density and highly accurate 3D point cloud of the TL corridor can be acquired [12], [13]. It can be used to accurately measure the distance between the TL and the ground objects in a TL corridor (especially trees and buildings) for power line safety distance detection, obstacle warning analysis or power line plane-section map drawing [2], [14], [15]. Numerous methods have been proposed for the extraction and reconstruction of TLs [16]–[20] based on point clouds acquired by airborne LiDAR. These mainly focus on modeling TLs from laser scanning data that have been acquired at a transient moment. For TL safety distance detection using point clouds, the main procedure used in conventional methods includes classification of the TL, reconstruction of the TL [21], [22], [29], and detection of the safety distance.

Previous methods described above are based on a data-driven approach, and most of them have strict requirements in terms of the original data. Specifically, good extraction results can be achieved when the point cloud density is high, while relatively poor results may be obtained when point cloud data are missing or when the point density is low. Furthermore, neither image-based methods nor LiDAR-based methods are able to detect the variations in the TL sag due to different weather conditions. Due to the influences of various factors, e.g. ambient temperature change, wind vibration and icing, the shape of TL and the distance from TLs to ground objects vary and this will threaten power grid security when the distance is too small [23], [24]. Therefore, it is essential to develop an effective approach predicting and modeling the dynamic changes in the TL shape according to actual conditions.

In this article, a TL modelling framework that can provide a simulated TL shape under different weather conditions is proposed in order to overcome the shortcomings of the instantaneously acquired laser scanning data. The main contributions of this work include: a TL simulation method is developed by combining the influence of weather conditions on the TL tension, the TL wire parameters and the 3D-description of the TL derived from point clouds, in order to simulate the TL shape under different operating states.

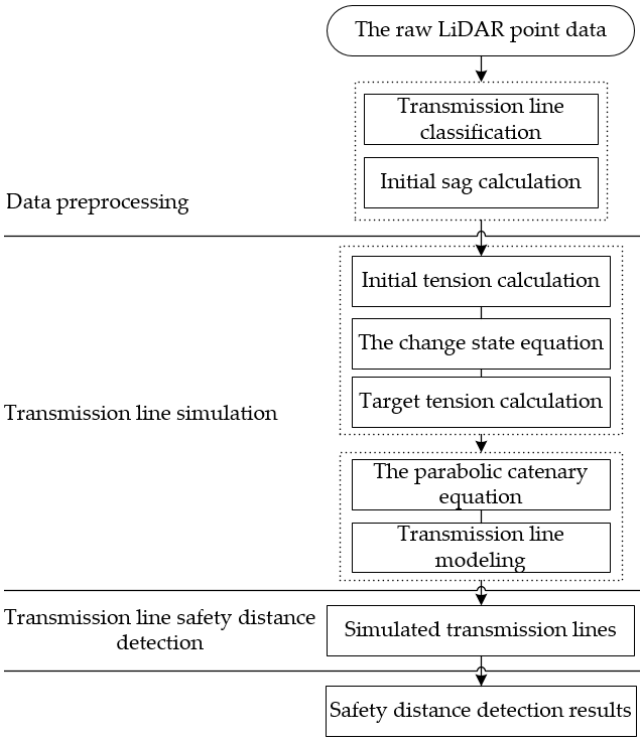

FIGURE 1. The framework proposed for transmission line simulation and warning.

The rest of this article is organized as follows: the proposed TL modelling framework is introduced in Section II-A. The simulation method is presented in detail in Section II-B. The experiment that was carried out to simulate the TLs under different weather conditions is introduced, and the verification of these results using laser scanning data is described in Section III. Some discussions about the proposed method are also given in this section. Lastly, Section IV gives the conclusions extracted from the work.

II. METHODS

Our TL simulation and warning procedure framework is composed of three stages as shown in Fig.1. First of all, data preprocessing for extracting TL points from raw point clouds and calculating the initial sag of TL. Next, the TL simulation based on mechanical computation. Finally, the TL safety distance detection after merging the simulated TL points into the point clouds.

A. SIMULATION ALGORITHM DESCRIPTION

Numerous studies have focused on identification and extraction of digital models of TLs from point clouds [14]–[22], but few studies has been devoted to elucidating how to use acquired data to provide some extra information to the TL operator. In this section, we proposed an overall description for the TL simulation combining the influence of weather conditions on the TL tension to provide supplemental information for TL risk assessment and warning along the corridor.

Sag and tension are the mechanical limiting factors for TL conductors [30]–[32]. Conductor elongate from initial

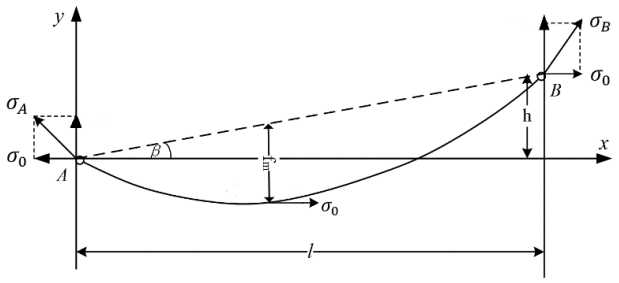

FIGURE 2. Sag and tensions in overhead transmission line span.

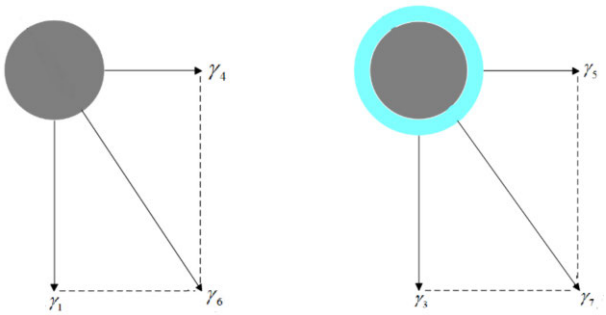

FIGURE 3. Force diagram for a TL in cross-section: (a) the self-gravity and wind-pressure load on the TL form a combined load; (b) vertical load due to ice coating and wind-pressure, forming a combined load. (color legend: wire - gray; ice - blue).

installation to a state of operation, because of temperature increase or working load increase (wind pressure, icing or their combinations). This elongation leads to increased sag. Sag is indirectly proportional to the tension applied to the conductor. Fig. 2 shows the sag and tensions in a TL span.

An overhead TL is suspended by two suspension points A and B of tower. The value of the horizontal component σ_0 of the tension of TL remains the same at any point on the TL, and equivalent to that of the tension at the lowest point of the TL. In the steady state, the horizontal tension σ_0 along the line section is constant and, therefore taking the horizontal tension as the basis for analyzing the force on the TL, such tension being uniform throughout any one span.

Sag primarily depends on the conductor type, length, weight, modulus of elasticity, temperature and tension [38], [39]. There is a relationship between these parameters, which can be expressed as the change-of-state equation of the overhead line [32], [33], [33]–[35]. The equation shows how the parameters relate to the transmission line sag under different weather conditions [36].

The shape of the TL catenary is approximately a parabolic curve when the overhead TL sags when suspended between two ends of tower supports. Hence, the parabolic catenary equation is used in this work to model the mechanical behavior of an overhead TL. Finally, the 3D shape of the TL under different working conditions can be calculated and modeled by the parabolic equation, combining the tension with the 3D position information for the suspension points.

B. PROPOSED APPROACH

1) DATA PREPROCESSING

The main purpose of data preprocessing is to obtain the initial sag for TL simulation, while classifying the LiDAR data of TL corridor for safety distance detection. Data preprocessing in our study consisted of three sub-steps: (1) classify the raw LiDAR point data into TL, pylon, vegetation and ground points using Terrasolid software; (2) identify the suspension points of TLs; (3) calculate the size of sag of each TL span according to the topological relation between point and line.

The sag of an overhead TL is defined as the vertical distance from the lowest points of the TL to the imaginary line connecting the two suspension points of the TL. Note that the precise identification of location of suspension point has an important effect on sag calculation. Thus, in order to obtain the highly precise location of suspension points, the points are manually identified by after-processing.

2) MECHANICAL STATE ESTIMATION

In this section, we focus on elaborating the TL tension related to TL simulation in different weather conditions. This process is composed of an initial tension calculation, a working load calculation and the tension calculation for the target state. A more detailed description of the three parts of is given as follows.

a: INITIAL TENSION CALCULATION

The tension in the TL vary in different weather conditions [30], [31]. The sag f_m of TL needs to be extracted from the point clouds firstly in order to calculate the tension at the moment of data acquisition by laser scanning; this is taken as the initial tension of the known states. The horizontal conductor tension can be calculated using Equation 1:

$$\sigma_0 = \frac{\gamma l^2}{8 f_m \cos\beta} \tag{1}$$

where σ_0 (units: N/mm^2) is the horizontal conductor tension, γ (units: N/m $\cdot$ mm^2) is the TL load, l (units: m) is the horizontal distance between conductor-insulator attachment points —span length, β (units: degree) is the elevation angle, fm (units: m) is the maximum sag in the TL derived from point clouds.

b: WORKING LOAD CALCULATION

The working load of a TL refers to the load per unit length and unit cross-sectional area. The TL load can comprise a variety of forces in the external and interior environment, as shown in Fig. 3.

The loads, γ, on a TL include the self-gravity, ice weight and wind pressure, which are generally considered as having a uniform distribution along the TL [32], [35]. Taking the load on the TL as a vector, the magnitude and direction of the load are different due to the TL's weight, the ice coating and the wind pressure. The different loads can be calculated as follows:

$$\text{Self-gravity load: } \gamma_1 = \frac{m_0 g}{A} \cdot 10^{-3} \tag{2}$$

$$\text{Ice weight load: } \gamma_2 = \frac{\rho_1 \pi b(b+d)g}{A} \cdot 10^{-3} \tag{3}$$

Load with ice coating: $\gamma_3 = \gamma_1 + \gamma_2$ (4)

Wind pressure load: $\gamma_4 = \frac{\rho_2 \alpha \mu d v^2 sin^2\theta}{2A} \cdot 10^{-3}$ (5)

Wind pressure load with ice coating:

$$\gamma_5 = \frac{\rho_2 \alpha \mu v^2 (2b + d) sin^2\theta}{2A} \cdot 10^{-3} \quad (6)$$

Combined load with wind: $\gamma_6 = \sqrt{\gamma_1^2 + \gamma_4^2}$ (7)

Combined load with wind and ice coating:

$$\gamma_7 = \sqrt{(\gamma_1 + \gamma_2)^2 + \gamma_4^2} \quad (8)$$

where, g is gravitational constant (units: m/s^2), m_0 is the weight per unit length (units: kg/km), A is the cross sectional area (units: mm^2), ice density ρ_1=0.9kg/m^3, standard air density ρ_2=1.25kg/m^3, b is the icing thickness (units: mm), d is the TL diameter (units: mm); α is the unevenness factor for the wind speed, and v is the wind speed (units: m/s), θ is the angle between the wind direction and the direction of TL. μ is the shape coefficient for the wind load: when the diameter of the TL is less than 17 mm, $\mu = 1.2$; when the diameter of the TL is greater than or equal to 17 mm, $\mu = 1.1$.

c: CALCULATION OF TENSION FOR THE TARGET

If the tension, the load and temperature for a given set of weather conditions are known, the tension for another set of weather conditions (target states) can be obtained using the change-of-state equation. The state equations are modeled using the relationship between sag, tension, elongated conductor length, and other conductor parameters [27]. The change-of-state equation for an overhead TL is formulated as

$$\sigma_n - \frac{E\gamma_n^2 l^2 \cos^3\beta}{24\sigma_n^2} = \sigma_1 - \frac{E\gamma_1^2 l^2 \cos^3\beta}{24\sigma_1^2} - \alpha E \cos\beta (t_n - t_1) \quad (9)$$

where α is the thermal elongation coefficient for the TL, E is the elasticity modulus, β is the elevation angle, σ_1 and σ_n are the horizontal tension in the TL for two different states, and γ and t are the TL load and temperature, respectively.

The change-of-state equation refers to the task of determining the unknown states from a given set of measurement and knowledge of the wire erosion over time using. The equation shows how the parameters relate to the TL sag under different weather conditions. The air temperature was employed for the change-of-state model. Considering the temperature difference value between measured condition and reference condition should be insensitive to the actual conductor temperature, the effect can be partially cancelled when both temperatures are similarly affected by these factors for the change-of-state equation.

3) TRANSMISSION LINE MODELING

According to the above-mentioned procedures, the tension of TL for target state was obtained using the sag-tension calculation. After the calculation, the TL shape can be simulated based on the parabolic catenary equation combining the tension. The parabolic catenary equation needs to be calculated under the given condition that the overhead TL is the compliant cable chain without stiffness, and the loads act on the TL and the temperature distributes uniformly along the length of TL. Based on this, the TL sag curve can be simulated easily. In this part, two kinds of sag curve case for TL modeling are considered, which are windless and windy condition.

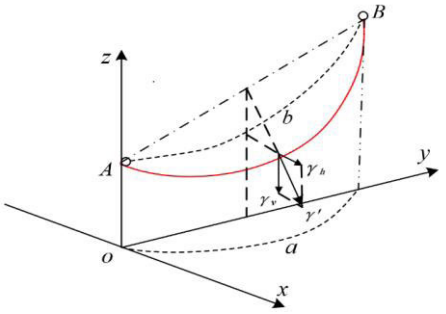

FIGURE 4. Transmission line lying in the deviated plane. (Curve a and Curve b is the projections of the TL in the horizontal plane and the vertical plane, respectively.)

a: TRANSMISSION LINE UNDER WINDLESS CONDITIONS

Under windless conditions, the only load on a TL is in the vertical direction. Assuming that the loads are uniformly distributed along the TL, the sag curve can be described as a function of the horizontal tension and weight per meter. In this work, a variant of the parabolic catenary equation was used to simulate the sag:

$$y = x \tan\beta - \frac{\gamma x(l - x)}{2\sigma \cos\beta} \quad (10)$$

In the above equation, l is the span length, γ is the load on the TL, σ is the tension corresponding to the target weather conditions, β the is vertical angle of the two suspension points in a span, and x is the horizontal distance from a given point on the TL to the suspension point.

b: TRANSMISSION LINE UNDER WINDY CONDITIONS

Under windy condition, there is both a vertical load, γ_v, and a horizontal load, γ_h, on a TL. And due to the horizontal load, the line rotates around the line joining the two suspension points. When the TL is subjected to a transverse force by the wind acting, a deviated plane is formed. In order to analyze the sag in the deviated plane, the sag curve is projected to both the vertical plane and the horizontal plane.

In the vertical projection plane, the inclined parabola formula of the TL for the wind deviation is

$$y_v = x \tan\beta - \frac{\gamma_v x(l - x)}{2\sigma \cos\beta} \quad (11)$$

In the horizontal projection plane, the height of the two suspension points is the same and the horizontal projection length of the inclined span, l_{AB}, is equal to actual span, l. The sag of the TL at any position in the horizontal projection plane is then described as:

$$y_h = \frac{\gamma_h x(l - x)}{2\sigma \cos\beta} \quad (12)$$

TABLE 1. Characteristics of point clouds of transmission lines corridors.

Dataset	Span 1	Span 2	Span 3
Point density	>55pts/m^2	>60pts/m^2	>32pts/m^2
Point number	1297983	3779536	3145456
Span length (m)	578	685	891
Pylons height difference (m)	28	68	113

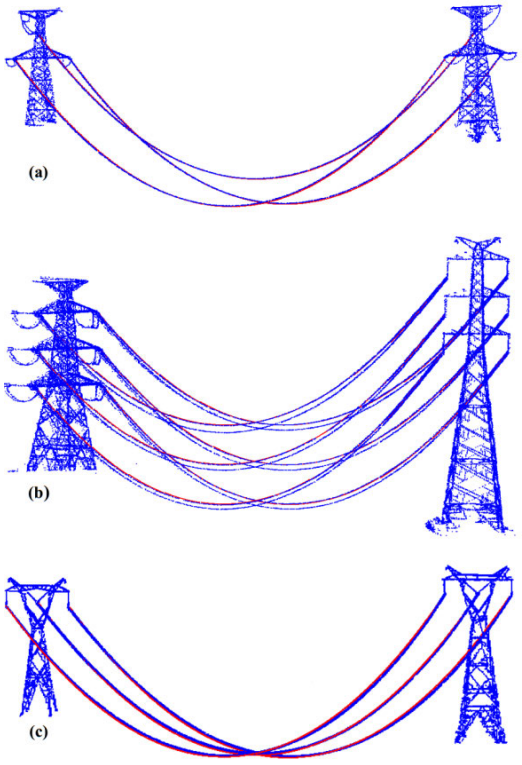

FIGURE 5. Transmission line simulation results. (a) Superposition of simulated TLs and scanned TL points from Span 1; (b) superposition of simulated TLs and scanned TL points from Span 2; (c) superposition of simulated TLs and scanned TL points from Span 3. (legend: original scanned transmission line and pylon points - blue; simulated transmission line points - red.)

III. RESULTS AND DISCUSSION

A. DATASETS AND EVALUATION METRICS

1) DATASETS

Our study site consisted of three overhead TL corridors under operation, 110kV, 220kV, 500kV, respectively, in Guangdong Province, southeast China. The point clouds data were acquired using Riegl VUX-1LR laser system (laser pulse rate: 50kHZ∼820kHZ, accuracy: 15mm, scanning range: 5m∼1350m) mounted on a large unmanned helicopter (payloads: 50kg∼80kg, endurance time: 4∼6h) with flying altitude AGL about 150m for TL cruising. From the three corridors data, we selected one testing span in each corridor and corresponding point clouds characteristics are shown in Tab. 1. The point clouds of the three TLs span are shown in Fig. 5.

The weather conditions were monitored on-line by the monitoring equipment installed on pylons in the corridors.

TABLE 2. Parameter of conductor and weather conditions.

Dataset	Span 1	Span 2	Span 3
Temperature(°C)	23.0	28.0	31.0
Wind speed(m/s)	1.0	2.0	3.0
Voltage level	110kV	220kV	500kV
Bundle conductors	1	2	4
Conductor type	LGJ-240/50	LGJ-240/50	LGJ-400/50

TABLE 3. Comparison of the experimental results obtained using Span 1.

Temperature(^{0}C)		23.0	
Wind speed(m/s)		1.0	
Layer of conductor	left	middle	right
Actual sag(m)	27.66	27.63	27.79
Simulated sag(m)	27.95	27.90	28.13
Bias(m)	0.29	0.27	0.34
D-Ratio(%)	1.05	0.98	1.22

Temperature and wind speed were the average in ten minutes. The weather conditions in the study area at the laser scanning time are shown in Tab. 2. Additionally, the conductor material type is GB1179-83 standard, China. Each span included three or six TLs. Each phase of the TL included one to four bundle conductors.

2) EVALUATION METRICS

To analyze the simulation results, the simulated TLs were compared with the original laser points. In order to evaluate the results of the simulation quantitatively, a map showing the deviation of X values and Z values from the 3D coordinates of the sampled TL was constructed. In addition, we used the following measure to evaluate the TL simulation results:

$$\text{Difference Ratio} = \frac{(SS) - (AS)}{(AS)} \tag{13}$$

where Actual Sag (AS) refers to the sag of TL as derived from the original point clouds and Simulated Sag (SS) is the sag of simulated TL obtained using the proposed method.

B. PERFORMANCE OF THE PROPOSED METHOD

In this section, we presented simulated results corresponding to the working conditions at the moment of the LiDAR data acquisition. Given one suspension point of a span as the starting point together with the sampled interval distance, e.g. 0.1 m, the 3D sag curves were modeled according to the proposed method; then the simulated TLs can then be output as 3D point clouds (see Fig.5). The amounts of sag in the lowest layers of each span were shown in Tabs 3∼5.

As shown in Fig.5, the red and blue TLs overlapped well, which the blue TLs are the original scanned TL points, and the red TLs are the simulated TL points corresponding to the working conditions at the moment of the data acquisition. From Tabs 3∼5, the sag bias of Span 1 was the least (0.34m), followed by Span 2 (0.47m) and Span 3 (0.65m). The difference ratios of the three spans were all less than 1.57%. The consistency between the original and the simulated TLs was overall satisfactory.

TABLE 4. Comparison of the experimental results obtained using Span 2.

Temperature(^{0}C)		28.0	
Wind speed(m/s)		2.0	
Layer of conductor	upper	middle	low
Actual sag(m)	31.75	32.05	32.14
Simulated sag(m)	32.16	32.43	32.61
Bias (m)	0.41	0.38	0.47
D-Ratio (%)	1.29	1.19	1.46

TABLE 5. Comparison of the experimental results obtained using Span 3.

Temperature(^{0}C)		31.0	
Wind speed(m/s)		3.0	
Layer of conductor	left	middle	right
Actual sag(m)	41.19	40.64	41.47
Simulated sag(m)	41.78	41.20	42.12
Bias(m)	0.59	0.56	0.65
D-Ratio(%)	1.43	1.38	1.57

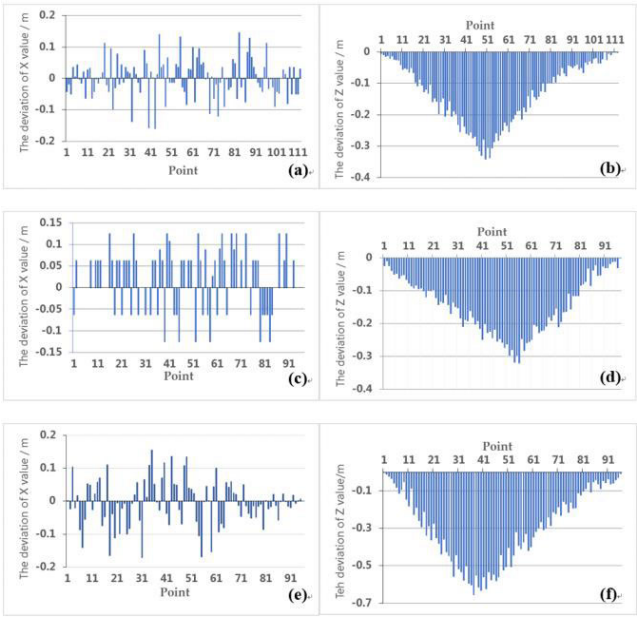

FIGURE 6. Comparison results of experimental and simulation results of X values and Z values. (a) and (b) Deviations of X and Z values from Span 1; (c) and (d) Deviations of X and Z values from Span 2; (e) and (f) Deviations of X and Z values from Span 3.

To accurately assess the performance of the proposed approach, the 3D point clouds of the simulated TL and the scanned TL were compared after sampled respectively according to the same distance interval along the TL. One TL of each span was selected for performance evaluation. Fig.6 shows the distribution of the deviation of the X and Z coordinate values of the sampled points of the three spans data.

As shown in Fig.6, the deviation of X values was relatively stable. The deviation in the value of X for the three spans ranged from −0.2m to 0.2m; the maximum deviations in Z for the three spans were less than 0.65m. The Data with maximum deviation in Z was Span 3 which has maximum span length and pylon height difference.

TABLE 6. Sag estimation data and results.

	Span 1		Span 2		Span 3	
Temperature (℃)	Tension (N/mm^2)	Sag (m)	Tension (N/mm^2)	Sag (m)	Tension (N/mm^2)	Sag (m)
-5	49.37	26.77	48.73	33.12	55.25	39.94
0	49.04	26.98	48.49	33.35	55.02	40.25
5	48.71	27.19	48.25	33.58	54.81	40.56
10	48.38	27.39	48.02	33.81	54.59	40.86
15	48.06	27.60	47.78	34.03	54.37	41.17
20	47.75	27.80	47.56	34.26	54.16	41.47
25	47.45	28.00	47.33	34.48	53.95	41.77
30	47.14	28.21	47.11	34.71	53.74	42.07
35	46.85	28.40	46.89	34.93	53.53	42.36
40	46.56	28.60	46.67	35.15	53.33	42.66

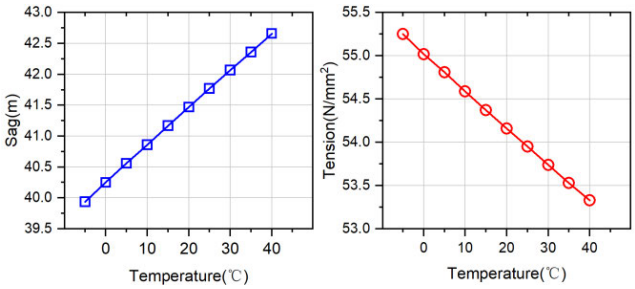

FIGURE 7. The dependency of (a) sag and (b) tension related with temperature.

C. SIMULATION RESULTS UNDER VARIOUS WORKING CONDITIONS

The sag estimation data and results for the three spans TLs under various working conditions were presented in Tab. 6. The temperature data for each set were shown in column 1 of the table. The estimated tensions were shown in columns 2, 4 and 6. The values of increased sag due to thermal effects (directly related to the temperature) evaluated at each measurement instant were also shown in columns 3, 5 and 7.

The sensitivities of tension and sag with respect to temperature were shown in Fig.7. This plot was obtained by using a set of varying temperature for Span 1. In the case of temperature variations, the transformation of the temperature to sag and tension appeared to be linear. It can be seen that the sag increased with the increase of temperature, whereas the tension decreased with the increase of temperature. This also indicated that the increase of temperature leads to the tension reduction and the extension of the TL length. This sensitivity analysis was an important because the temperature was the critical parameter under windless working conditions in the state estimation process.

The wind speed estimation data and results for the three spans TLs were presented in Tab. 7. The simulated wind speed data for each set were shown in column 1 of the table. The transverse tensions were shown in columns 2, 4 and 6. The values of increased tension due to wind pressure (directly related to the wind speed) evaluated at each measurement instant were also shown in columns 3, 5 and 7.

TABLE 7. Sag estimation data and results.

	Span 1		Span 2		Span 3	
Wind speed (m/s)	Transverse tension (N/mm^2)	Tension (N/mm^2)	Transverse tension (N/mm^2)	Tension (N/mm^2)	Transverse tension (N/mm^2)	Tension (N/mm^2)
5	2.03	51.38	2.02	51.27	1.84	57.49
10	8.13	52.24	8.06	51.84	7.37	57.92
15	13.70	53.33	13.59	52.94	12.42	58.74
20	19.77	55.11	19.63	54.73	17.94	60.10
25	30.73	59.70	30.56	59.37	27.97	63.69
30	43.90	67.12	43.75	66.89	40.11	69.69
35	59.10	77.56	59.06	77.51	54.27	78.46

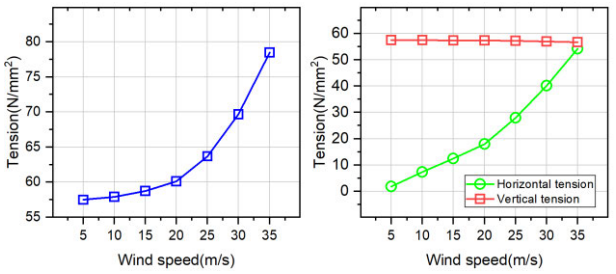

FIGURE 8. The characteristics of the tensions dependency on the wind speed.

The sensitivities of tensions with respect to the wind speed were shown in Fig.8. This plot was obtained by using a set of varying wind speeds and their corresponding tensions for Span 1. Given the wind direction is perpendicular to the TL along the horizontal direction. It was demonstrated in Fig.8 that the tension varies with the increased wind speed. The vertical tension remained unvaried due to the unchanged self-weight of the TL. The horizontal tension perpendicular to the TL increased with the increase of wind pressure. This sensitivity analysis was also important because the wind speed was the critical parameter under windy working conditions in the state estimation process.

Thus, the sag computation based on a nonlinear state estimation model captured gradual sag level increases. This would enable the operator to know the potential encroaching points in TL corridors based on safety distance detection and to take appropriate counter measures to avoid further clearance violations and cascading failures. The varied tension measurements also verified the accuracy of the TL state estimation process. Although there is no access to actual measurements on TL under extreme working conditions is available, we have verified our method through an indirect approach. The sensitivity analysis about varied tension measurements verified the accuracy of the TL state estimation approach. The increase in sag levels due to reduced tension values were provided to verify the accuracy of the TL simulation method.

1) APPLICATION OF SIMULATION UNDER EXTREME WORKING CONDITIONS

In this section, we primarily focus on simulating TLs under extreme working conditions. The main aim of the proposed method is to merge the simulated transmission line points into the point clouds of TL corridor and to calculate the distance between object points and the simulated TL. If the distance between tree or building points to the TL does not meet the safety regulations requirements, the points are identified as potential encroaching points. This can provides the more information for TL inspection and maintenance so that the

TABLE 8. Comparison of original sag and simulated sag under typical climatic conditions.

State	Condition	Original sag(m)	Variation (m)
Original state	23^{0}C	28.08	0
Maximum temperature	40 ^{0}C	29.89	1.81
Minimum temperature	-5 ^{0}C	26.92	-1.16
Maximum wind	35m/s	-	3.75

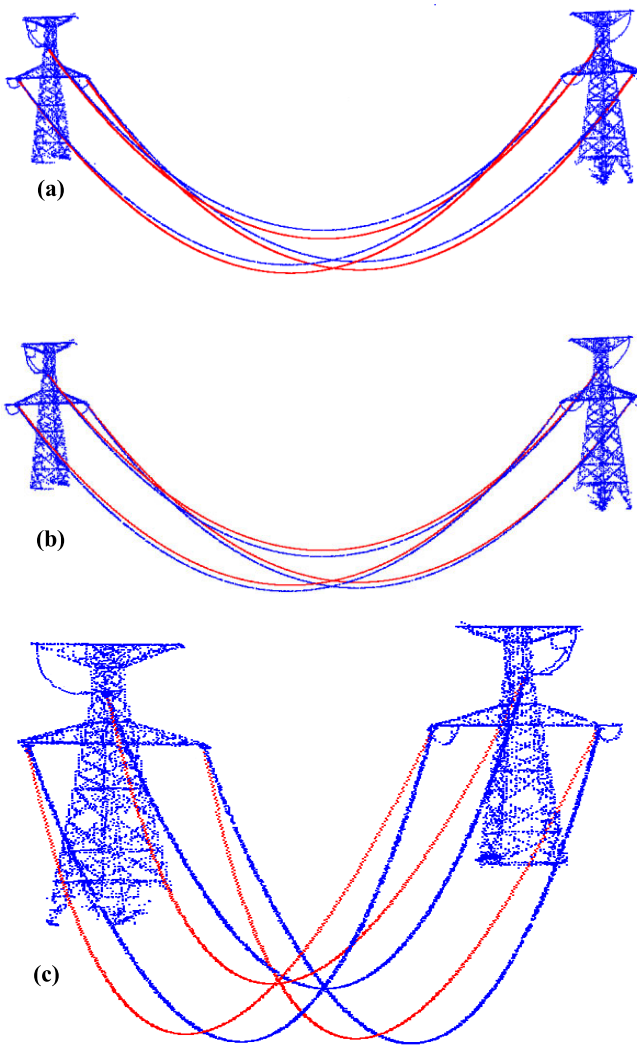

FIGURE 9. Superposition of original scanned transmission lines and simulated transmission lines under extreme weather conditions. (temperature: t, wind speed: v, ice thickness: b). (a) Extreme high temperatures (t=40°, v=0m/s, b=0mm); (b) Extreme low temperatures (t=−20°,v=0m/s, b=0mm); (c) Extreme high wind speed(t=10°, v=35m/s, b=0mm).

operator can quickly search for, locate and eliminate the risk objects at the scene. In extreme weather conditions, TLs can be affected seriously and there is a higher possibility for a serious power failure to occur. Therefore, it is important to estimate TLs under various extreme weather conditions.

Taking Span 1 as an example, the three kinds of TL shape can be obtained using the TL simulation method described earlier. The original TLs collected by airborne LiDAR were used as a reference to calculate the sag variation. The results were shown in Tab.8. Fig.9 shows the contrast between the original TLs points and the simulated TLs: the blue curve is formed from the original TLs points whereas the red curves show the simulated TLs.

The three spans are located within Meteorological Area I of the nine typical Meteorological Areas of China. In the Meteorological Area, the air temperatures corresponding to three typical extreme weather conditions – i.e., maximum temperature, minimum temperature and maximum wind speed–are 40°C, -5°C and 10°C, respectively. The maximum wind speed, v, is $35m/s$. Note that the maximum ice coating thickness, b, is $0mm$ in the Meteorological Area I. Three kinds of typical extreme weather conditions in the study area are considered: extreme high temperatures, extreme low temperatures and extreme high wind speed.

In the case of extreme temperature variations, the transformation of the temperature to sag appeared to be obvious. It can be seen that the sag increased with the increase of temperature, whereas the sag reduced with the decrease of temperature (see Figs. 9a & 9b). In the case of windy conditions, there is a load on the TL due to the wind acting coupled with self-gravity. The TL will then deviate from the vertical plane and rotate around the line connecting the two suspension points. Assuming the wind direction is perpendicular to the TL along the horizontal direction, the simulated results for extreme high wind speed were shown in Fig. 9c. The maximum deflection value of the TL in the transverse direction was 3.75m.

IV. CONCLUSION

This article provides an approach for TL simulation based on mechanical computation for risk analysis using point clouds. Different from traditional methods, which directly detect dangerous ground objects based on the LiDAR point clouds, our approach provides TLs sag under the extreme weather conditions which is difficult to acquire by the means of airborne LiDAR remote sensing technology. The proposed approach combined with point clouds and weather parameters is carried out in order to provide early warning of encroaching objects along TL corridors. The simulated TLs under extreme weather conditions can be combined with TL safety distance detection to assess potential encroaching objects. This provides a scientifically sound simulation approach for TL safety distance assessment and warning along the corridor.

The performance of the proposed approach was evaluated and visualized with three span TLs dataset. The accuracies of Span 1 were the highest (i.e., the deviation in Z values: 0.34m, D-Ratio: 1.22%), followed by Span 2 (i.e., the deviation in Z values: 0.47m, D-Ratio: 1.46%) and Span 3 (i.e., the deviation in Z values: 0.65m, D-Ratio: 1.57%). The results suggested that the TL simulation method is effective to simulate the 3D shape of TL. These results also provide a quantifiable basis for TL simulation in the safety distance detection processing chain. Besides, we have demonstrated the potential of TL simulation under various working conditions particularly for extreme weather condition. The sensitivity analyses were preformed to estimate the variation of sag and tension with respect to temperature and wind speed. The results showed that the sag computation based on a nonlinear state estimation model captured gradual sag level increases. This could provide an indirect approach to verify the state estimation model. However, there are still some limitations in TL simulation, especially for TLs with long span length and large pylons height difference. Future studies are required for TL simulation, particularly on combining measurement and input parameters as mentioned in this work to improve the accuracy of larger span TL simulation. In addition, tree growth, which significantly influences the detection of potential risk points, especially during the growing season or during the interval between cruising flights, will be considered in order to improve the risk analysis results.

REFERENCES

[1] B. Guo, Q. Li, X. Huang, and C. Wang, "An improved method for power-line reconstruction from point cloud data," *Remote Sens.*, vol. 8, no. 1, p. 36, Jan. 2016.
[2] S. J. Mills, M. P. Gerardo Castro, Z. Li, J. Cai, R. Hayward, L. Mejias, and R. A. Walker, "Evaluation of aerial remote sensing techniques for vegetation management in power-line corridors," *IEEE Trans. Geosci. Remote Sens.*, vol. 48, no. 9, pp. 3379–3390, Sep. 2010.
[3] L. Matikainen, M. Lehtomäki, E. Ahokas, J. Hyyppä, M. Karjalainen, A. Jaakkola, A. Kukko, and T. Heinonen, "Remote sensing methods for power line corridor surveys," *ISPRS J. Photogramm. Remote Sens.*, vol. 119, pp. 10–31, Sep. 2016.
[4] J. Ahmad, A. S. Malik, L. Xia, and N. Ashikin, "Vegetation encroachment monitoring for transmission lines right-of-ways: A survey," *Electr. Power Syst. Res.*, vol. 95, pp. 339–352, Feb. 2013.
[5] A. Albert and M. R. Hallowell, "Safety risk management for electrical transmission and distribution line construction," *Saf. Sci.*, vol. 51, no. 1, pp. 118–126, Jan. 2013.
[6] S. Ashidate, S. Murashima, and N. Fujii, "Development of a helicopter-mounted eye-safe laser radar system for distance measurement between power transmission lines and nearby trees," *IEEE Trans. Power Del.*, vol. 17, no. 2, pp. 644–648, Apr. 2002.
[7] M. Frank, Z. Pan, B. Raber, and C. Lenart, "Vegetation management of utility corridors using high-resolution hyperspectral imaging and LiDAR," in *Proc. 2nd Workshop Hyperspectral Image Signal Process., Evol. Remote Sens.*, Jun. 2010, pp. 14–16.
[8] S. Clode and F. Rottensteiner, "Classification of trees and powerlines from medium resolution airborne laserscanner data in urban environments," in *Proc. APRS Work Digit. Image Comput.*, Feb. 2005, pp. 191–196.
[9] G. Yan, C. Li, G. Zhou, W. Zhang, and X. Li, "Automatic extraction of power lines from aerial images," *IEEE Geosci. Remote Sens. Lett*, vol. 4, no. 3, pp. 387–391, Jul. 2007.
[10] C. L. Glennie, W. E. Carter, R. L. Shrestha, and W. E. Dietrich, "Geodetic imaging with airborne LiDAR: The Earth's surface revealed," *Rep. Prog. Phys. Phys. Soc.*, vol. 76, no. 8, Jul. 2013, Art. no. 086801.
[11] M. L. Lu and Z. Kieloch, "Accuracy of transmission line modeling based on aerial LiDAR survey," *IEEE Trans. Power Del.*, vol. 23, no. 3, pp. 1655–1663, Jul. 2008.

[12] H. Guan, Y. Yu, J. Li, Z. Ji, and Q. Zhang, "Extraction of power-transmission lines from vehicle-borne lidar data," *Int. J. Remote Sens.*, vol. 37, no. 1, pp. 229–247, Jan. 2016.

[13] H. B. Kim and G. Sohn, "Point-based classification of power line corridor scene using random forests," *Photogramm. Eng. Remote Sens.*, vol. 79, no. 9, pp. 821–833, Sep. 2013.

[14] B. Guo, X. Huang, Q. Li, F. Zhang, J. Zhu, and C. Wang, "A stochastic geometry method for pylon reconstruction from airborne LiDAR data," *Remote Sens.*, vol. 8, no. 3, p. 243, Mar. 2016.

[15] M. Ritter and W. Benger, "Reconstructing power cables from LiDAR data using eigenvector streamlines of the point distribution tensor field," in *Proc. Int. Comput. Graph., Visual. Comput. Vis.*, Jun. 2012, pp. 25–28.

[16] T. Melzer *et al.*, "Extraction and modeling of power lines from air-borne point clouds," in *Proc. Work Pattern Recognit.*, Jun. 2004, pp. 47–54.

[17] R. A. Mclaughlin, "Extracting transmission lines from airborne LIDAR data," *IEEE Geosci. Remote Sens. Lett.*, vol. 3, no. 2, pp. 222–226, Apr. 2006.

[18] Y. Jwa and G. Sohn, "A piecewise catenary curve model growing for 3D power line reconstruction," *Photogramm. Eng. Remote Sens.*, vol. 78, no. 12, pp. 1227–1240, Dec. 2012.

[19] G. Sohn, Y. Jwa, and H. B. Kim, "Automatic powerline scene classification and reconstruction using airborne LIDAR data," in *Proc. ISPRS Ann. Photogram. Remote Sens. Spatial Inf.*, Jan. 2018, pp. 167–172.

[20] L. Cheng, L. Tong, Y. Wang, and M. Li, "Extraction of urban power lines from vehicle-borne LiDAR data," *Remote Sens.*, vol. 6, no. 4, pp. 3302–3320, Apr. 2014.

[21] B. Conde, A. Villarino, M. Cabaleiro, and D. Gonzalez-Aguilera, "Geometrical issues on the structural analysis of transmission electricity towers thanks to laser scanning technology and finite element method," *Remote Sens.*, vol. 7, no. 9, pp. 11551–11569, Sep. 2015.

[22] W. Liao, F. Van Coillie, L. Gao, L. Li, B. Zhang, and J. Chanussot, "Deep learning for fusion of APEX hyperspectral and full-waveform LiDAR remote sensing data for tree species mapping," *IEEE Access*, vol. 6, pp. 68716–68729, 2018.

[23] Y. Jaw and G. Sohn, "Wind adaptive modeling of transmission lines using minimum description length," *ISPRS J. Photogramm. Remote Sens.*, vol. 125, pp. 193–206, Mar. 2017.

[24] M. Muhr, S. Pack, S. Jaufer, W. Haimbl, and A. Messner, "Experiences with the weather parameter method for the use in overhead line monitoring systems," *Elektrotechnik Informationstechnik*, vol. 125, no. 12, pp. 444–447, Dec. 2008.

[25] S. M. Meng, W. Kong, and B. Tang, *Design of Overhead Transmission Line*, 2th ed. Beijing, China: China Electric Power Press, 2007, pp. 50–99.

[26] J. J. Huang, "Method to improve accuracy of sag measurement for transmission line using computer software," *Electr. Power Construct.*, vol. 25, pp. 27–30, 2004.

[27] D. S. Zhang, *Design Manual for High Voltage Transmission Line of Electric Power Engineering*, 2nd ed. Beijing, China: China Electric Power Press, 2003, pp. 82–95 and 166-212.

[28] Z. J. Liu, J. Liang, and J. X. Zhang, "Power lines extraction from airborne LiDAR data using spatial domain segmentation," *J. Remote Sens*, vol. 18, pp. 61–76, 2014.

[29] X. G. Lin *et al.*, "3D power line reconstruction from airborne LiDAR point cloud of overhead electric power transmission corridors," *Acto Geodaetica Cartographica Sinica*, vol. 45, pp. 347–353, Mar. 2016.

[30] M. Keshavarzian and C. H. Priebe, "Sag and tension calculations for overhead transmission lines at high temperatures-modified ruling span method," *IEEE Trans. Power Del.*, vol. 15, no. 2, pp. 777–783, Apr. 2000.

[31] E. Lindberg, *The Overhead Line Sag Dependence on Weather Parameters and Line Current*. Uppsala, Sweden: Uppsala Univ., 2011.

[32] I. Albizu, A. J. Mazon, and E. Fernandez, "A method for the sag-tension calculation in electrical overhead lines," *Int. Rev. Electr. Eng.*, vol. 6, no. 3, pp. 1380–1389, 2011.

[33] CIGRÉ B2-12 Technical Brochure. *Sag-Tension Calculation Methods for Overhead Lines*. Accessed: 2007. [Online]. Available: http://e-cigre.org/publication/324-sag-tension-calculation-methods-for-overhead-lines

[34] B. David *et al.*, "Predicting the conductor sag of power lines in a new model of dynamic line rating," *Proc. Elect. Insul.*, pp. 7–10, Jun. 2015.

[35] C. O. Boyse and N. G. Simpson, "The problem of conductor sagging on overhead transmission lines," *J. AIEE*, vol. 91, no. 48, pp. 219–231, Dec. 1944.

[36] I. Albizu, A. J. Mazon, and I. Zamora, "Flexible strain-tension calculation method for gap-type overhead conductors," *IEEE Trans. Power Del.*, vol. 24, no. 3, pp. 1529–1537, Jul. 2009.

[37] H. Keyhan, G. McClure, and W. G. Habashi, "Dynamic analysis of an overhead transmission line subject to gusty wind loading predicted by wind–conductor interaction," *Comput. Struct.*, vol. 122, pp. 135–144, Jun. 2013.

[38] A. Polevoy, "Impact of data errors on sag calculation accuracy for overhead transmission line," *IEEE Trans. Power Del.*, vol. 29, no. 5, pp. 2040–2045, Oct. 2014.

[39] P. Ramachandran, V. Vittal, and G. T. Heydt, "Mechanical state estimation for overhead transmission lines with level spans," *IEEE Trans. Power Syst.*, vol. 23, no. 3, pp. 908–915, Aug. 2008.

[40] M. T. Bedialauneta, I. Albizu, E. Fernandez, A. J. Mazon, and S. de Arriba, "Monitoring the tension and the temperature in an overhead line," in *Proc. 16th IEEE Medit. Electrotechnical Conf.*, Mar. 2012, pp. 245–248.

[41] D. Balangó, B. Nemeth, and G. Gocsei, "Predicting conductor sag of power lines in a new model of dynamic line rating," in *Proc. IEEE Electr. Insul. Conf. (EIC)*, Aug. 2015, pp. 7–10.

[42] I. Theodosoglou, V. Chatziathanasiou, A. Papagiannakis, B. Więcek, and G. De Mey, "Electrothermal analysis and temperature fluctuations' prediction of overhead power lines," *Int. J. Electr. Power Energy Syst.*, vol. 87, pp. 198–210, May 2017.

[43] I. Albizu, A. J. Mazon, V. Valverde, and G. Buigues, "Aspects to take into account in the application of mechanical calculation to high-temperature low-sag conductors," *IET Gener., Transmiss. Distrib.*, vol. 4, no. 5, pp. 631–640, May 2010.

[44] F. Passerini and A. M. Tonello, "Smart grid monitoring using power line modems: Effect of anomalies on signal propagation," *IEEE Access*, vol. 7, pp. 27302–27312, Feb. 2019.

[45] Q. Li, Y. Zhang, T. Ji, Z. Liu, C. Li, Z. Cai, and P. Yang, "Robust optimal reactive power dispatch with feedback and correction against uncertainty of transmission line parameters," *IEEE Access*, vol. 6, pp. 39452–39465, Jul. 2018.

[46] L. Changchao, K. Zhongjian, Y. Hongguo, R. Kihong, and Z. Shichao, "Identifying the key transmission lines considering the power flow impact force," *IEEE Access*, vol. 7, pp. 96297–96308, Jul. 2019.

SAI CHANG ZHANG received the M.S. degree in photogrammetry and remote sensing from the Chinese Academy of Surveying and Mapping, in 2018. He is currently pursuing the Ph.D. degree in cartography and geographical information system with the University of Chinese Academy of Sciences.

His research interests include power line inspection of airborne LiDAR and hyperspectral LiDAR in remote sensing application.

JUN ZHENG LIU received the Ph.D. degree in cartography and geographical information system from the Institute of Remote Sensing and Digital Earth, Chinese Academy of Sciences, in 2003.

He is currently a Professor with the Chinese Academy of Surveying and Mapping. He is the author of two books and more than 67 articles. His research interests include power line inspection of airborne LiDAR, remote sensing image change detection, and mapping application of LiDAR and multisensory fusion.

ZHENG NIU received the B.S. and M.S. degrees in geophysical engineering from Peking University and the Ph.D. degree in physical geography from the Institute of Geographic Sciences and Natural Resources, Chinese Academy of Sciences, in 1996.

He is currently a Research Professor with the Aerospace Information Research Institute, Chinese Academy of Sciences. He is the author of three books and more than 120 articles. His research interest includes environmental remote sensing.

SHUAI GAO received the Ph.D. degree in cartography and geographic information system from the University of Chinese Academy of Sciences, Beijing, China, in 2011. He is an Associate Research Fellow with the Aerospace Information Research Institute, Chinese Academy of Sciences. His research interests include remote sensing modeling of radiative transfer, LiDAR remote sensing, machine learning, and spatial data mining.

HAI ZHI XU received the B.S. degree in electrical engineering and automation from Shanghai Jiao Tong University and the Ph.D. degree in electrical engineering from Tsinghua University, in 2006.

He is currently a Senior Engineer at China Southern Power Grid. His research interests include the power line inspection of airborne LiDAR and mapping application of multisensory fusion.

JIE PEI received the B.S. degree in geographic information system from the Hefei University of Technology and the Ph.D. degree in cartography and geographic information system from the University of Chinese Academy of Sciences, in 2020.

He is currently an Assistant Professor Fellow with the School of Geospatial Engineering and Science, Sun Yat-Sen University. His research interests include the environmental change detection and attribution using time-series remotely sensed imagery and other geospatial data.